Available on CMS information server **CMS IN 2004/035**

CMS Internal Note

The content of this note is intended for CMS internal use and distribution only

September 27, 2004

Some results on the DT Local Muon trigger performance from the 2003 Testbeam

J. Caballero, M. Cerrada, N. Colino, B. de la Cruz, C. Fernández, M.C. Fouz, M.I. Josa, J. Puerta, L. Romero, C. Villanueva, C. Willmott

CIEMAT, Madrid, Spain

J. Fernández de Trocóniz

Universidad Autónoma de Madrid, Madrid, Spain

Abstract

In May 2003 a MB3 chamber was exposed to a structured muon LHC-like beam with the goal of performing a full test of the DT local muon trigger. The results were very satisfactory and a summary of them have been submitted to Nuclear Instruments and Methods for publication. We present in this note a more detailed view of some of the results. Our approach has been to start from the information provided by the chamber readout TDC's and use it to test the trigger performance.

1 Introduction

A MB3 DT chamber was exposed during May 2003 to a muon beam with a LHC-like structure at the H6 CERN SPS North Area. The aim of the test was to make a full check of the different components of the local muon trigger system (BTI-TRACO-TS), both from the hardware and the software point of view.

A full description of the trigger system and the experimental setup used as well as most relevant results can be found in [1].

Since the chamber could be rotated around a vertical axis, we are able to study the effect of the incident muon beam hitting the chamber with several angles of incidence. In the test beam configuration, the θ superlayer was not affected by the rotation, while superlayers SL-ϕ_1 and SL-ϕ_2 and the corresponding trigger elements are sensitive to it. Data were taken at different angles and with different trigger configurations.

In this Note we present some results, only partially included in [1], from the analysis of the test beam data. From the physics point of view, the trigger system should be able to efficiently trigger on every muon susceptible to be detected in CMS. To check this, muons efficiently reconstructed by the muon chamber are first considered and then used to study the trigger system performance. A complementary approach, which we have not followed here, would be to compare the data with expectations from a trigger emulation algorithm [1]. In this Note we make emphasis in the physics point of view.

The trigger system and the offline track reconstruction use the same information, namely the one from the hits recorded in the DT cells. The BTI combines the drift times collected in the four layers of a superlayer and delivers a High Quality Trigger when a good alignment of 4 hits is achieved. If only three hits are properly aligned the trigger is marked as a Low Quality Trigger. Ideally, one may expect that a High Quality Trigger is equivalent, at the Superlayer level, to a 4-hit reconstructed track (1 hit per Layer in all four Layers of the SL). Similarly, a Low Quality trigger can be assimilated, at the Superlayer level, to a 3-hit reconstructed track (1 hit per Layer in only 3 Layers of the Superlayer).

In the $r-\phi$ view two superlayers per chamber are available. Therefore two track segments reconstructed in the chamber can be obtained for the same muon. The trigger information from the two BTIs is sent to the TRAck COrrelator (TRACO) that combines it deliverying a more accurate information already at the trigger level. Again, a correspondence between trigger output and track reconstruction may be expected.

The organization of this Note is the following: in Section 2 a track reconstruction algorithm is established to optimize the agreement between the reconstruction at the trigger and detector levels. In Section 3 we present results on the trigger performance first in the $r-\phi$ view, and second in the θ view. In Section 4 some results on di-muon trigger efficiency are reported. Finally, in Section 5 studies on ghost triggers are presented. Conclusions are drawn in Section 6.

We present results from data taken with the muon beam hitting the chamber at the following nominal angles:

- Negative angles: -10, -20, -30 degrees.
- Positive angles: 0, 5, 10, 15, 20, 25, 30, 35, 45 degrees.

Muon tracks reconstructed in the chamber, as explained in the next section, were used to measure the incident beam angle, and the correspondance between the nominal beam angle and the actual one measured from the muons themselves is shown in Table 1.

Each run contained typically 10^5 events. All runs analysed correspond to the **default trigger** configuration.

In the following tables and figures, values from runs with positive and negative incident angles are interleaved according to the absolute value of the angle, since the results have proven to be independent of the sign of the angular displacement, as expected.

Run number	591	566	496	372	609	331	610	393	621	409	622	623
Nominal Angle (deg)	-30	-20	-10	0	5	10	15	20	25	30	35	45
Real angle (deg) ($\pm 2 \times 10^{-3}$ deg)	-28.8	-20.1	-10.7	-0.3	5.9	11.3	14.1	19.1	20.9	30.9	32.6	42.5

Table 1: Correspondance between the nominal and the real beam incident angle, measured from the muon tracks reconstructed in the DT chamber.

2 Track reconstruction algorithm

The chamber was calibrated and aligned following the procedure established in [2]. Details on results from calibration and alignment at different angles of incidence were reported in [3].

Muon tracks are reconstructed from the hits in each superlayer, minimizing the χ^2 of the fit to straight segments. All possible fits with 3 and 4 hits are tried. At LHC, one will often prefer a good fit with 3 hits from a bad 4-hit fit. Therefore 4-hit fits are required to have a χ^2 smaller than a given threshold value. If a 4-hit fit has a χ^2 bigger than this value, it is assumed that the fit is picking a bad hit. The bad hit is identified as the one contributing more to the χ^2, and removed from the fit, and a 3-hit fit is then tried.

In fact, what it is used as the figure of merit of the track is the sum of the squared residuals of the hit positions to the fitted track, and therefore has dimension of length squared. To become the standard χ^2 one has to divide it by the resolution squared. One can take our definition as the standard χ^2 for a pseudo-resolution of 1 mm.

The only free parameter of this algorithm is the threshold χ^2. We let the trigger system fix this value, in such a way that the agreement between trigger and detector response is maximum.

We start with the θ view as there is only one Superlayer providing information on this coordinate plane. Trigger information in this case is provided only by the BTI. Events with a single 4-hit track are selected. Figure 1 shows the χ^2 distribution for these selected tracks. Events are splitted into three samples: events with High Quality trigger (H), events with Low Quality trigger (L), and events with no trigger. From the figure it is clear that, as expected, the trigger quality is strongly correlated with the fit-χ^2. High Quality triggers have low values of the fit-χ^2 whereas Low Quality triggers have relatively larger values of the χ^2. The value of $\chi^2 = 2\ \mathrm{mm}^2$ seems to be the separation border between both regions. In the $r-\phi$ view two superlayers are available and two track segments can be reconstructed. A sample of events having one 4-hit fit in SL-ϕ_1 and in SL-ϕ_2 is selected. A High Quality trigger, that is HH, is expected for these events. Figure 2, left, shows the maximal χ^2 distribution (max[$\chi^2(\phi_1)$, $\chi^2(\phi_2)$]) for the run taken at normal incidence.

Again, a very strong correlation is observed between the trigger quality and the fit-χ^2. High Quality triggers have low values of the fit-χ^2 and Low Quality triggers have relatively larger values of the χ^2. Again, the value of $\chi^2 = 2\ \mathrm{mm}^2$ seems to be the separation border between both regions.

The argument also holds for the case of non-normal incidence. Figure 2, right, shows the maximal χ^2 distribution for 20° and Figure 3 shows the maximal χ^2 distribution for the runs taken at -30° and 30°. In all cases a cut at $\chi^2 \sim 2\ \mathrm{mm}^2$ efficiently separates the High Quality and the Low Quality trigger regions.

One has to notice that -30° angle is, in fact, -28.8° and 30° is 30.9° (see Table 1), and in this latter case the fraction of events with low χ^2 but with Lower Quality trigger starts to be significant.

Figures 1, 2 and 3 confirm that there is a correlation between a High Quality trigger, and a good 4-hit fit (with $\chi^2 < 2\ \mathrm{mm}^2$), at the DT chamber level.

In conclusion, in the following of the note, we will use the track fitting algorithm with a cut at $\chi^2 = 2\ \mathrm{mm}^2$.

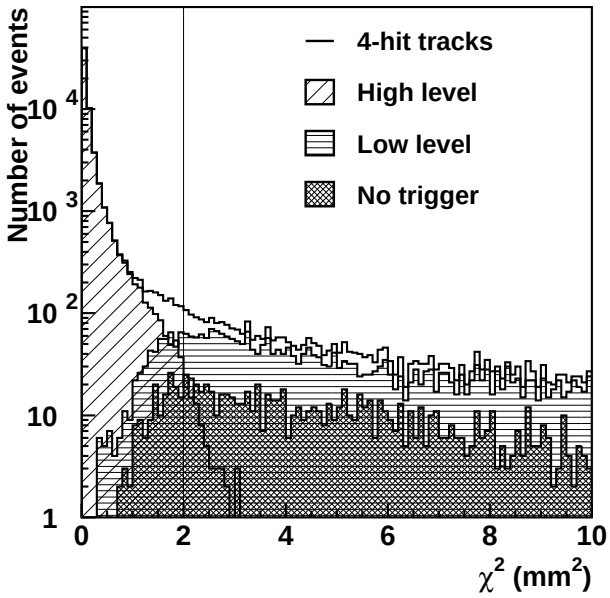

Figure 1: χ^2 distribution for events having only one 4-hit fit in the θ superlayer (Run 372).

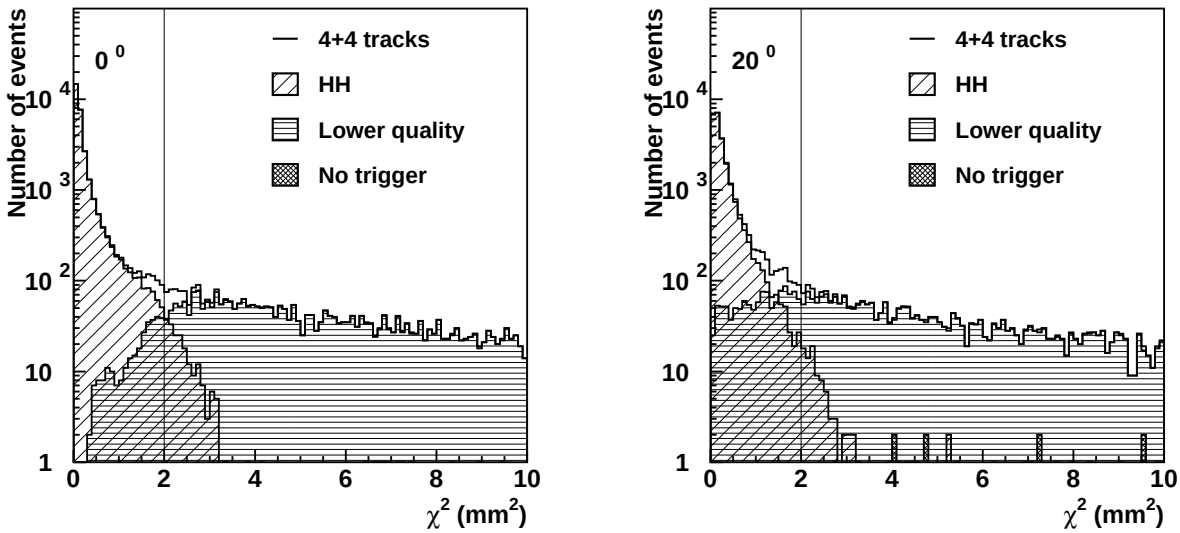

Figure 2: Maximal χ^2 distribution for events having one 4-hit fit in SL-ϕ_1 and in SL-ϕ_2. The left plot is for normal incidence (Run 372), the right one is for an angle of incidence of 20 degrees (Run 393).

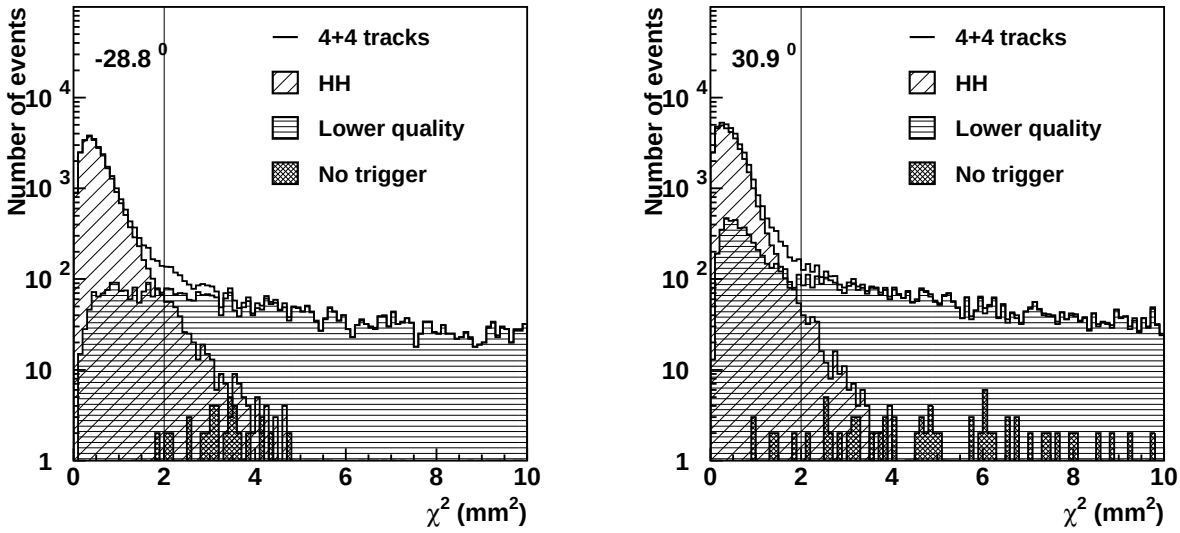

Figure 3: Maximal χ^2 distribution for events having one 4-hit fit in SL-ϕ_1 and SL-ϕ_2. The left plot is for an angle of incidence of -30 degrees (Run 591) and the right one is for +30 degrees (Run 409).

3 Single-muon trigger performance

To ensure that the muon reconstructed in the chamber and the one providing the trigger is the same, we select events having only one fit in the relevant Superlayer(s) (labelled **single-fit** events). Events with more than one track segment reconstructed in a given superlayer are generally due to more than one muon crossing the chamber at the same time. Considering these events complicates the analysis without improving the statistical significance of the results.

Two subsamples are investigated: events with only one hit in the cells participating in the fit (labelled as **single-hit** fits), and events with more than one hit collected in a cell participating in the segment fit (labelled as **multi-hit** fits). Multi-hit fits usually have a physical origin (emission of delta-rays).

Unlike the DT chamber, the trigger system is only able to process the first hit collected at the wire. In the multi-hit case, it may happen that the signal pattern received by the trigger be distorted if the first hit collected does not come from the real muon crossing the cell, but from a secondary emission. This may result in a decrease of the trigger efficiency.

The fraction of events with single-hit fits in the $r-\phi$ view is $(55.1 \pm 2.6)\%$ of the single-fit sample.

3.1 ϕ Superlayers

A single muon event is defined to be an event with at most one track segment fitted in SL-ϕ_1 and in SL-ϕ_2. The single-muon sample can be splitted into different cathegories depending on the number of hits participating in the fit:

- Sample **4+4**: A 4-hit fit in each ϕ superlayer (ϕ_1 and ϕ_2).
- Sample **4+3**: A 4-hit fit in one ϕ superlayer and a 3-hit fit in the other.
- Sample **3+3**: A 3-hit fit in both ϕ superlayers.

One has to notice that the sample **4+3** includes both "true" 4+3 tracks, in the sense than only 3 hits are collected in one superlayer, plus cases where 4 hits are collected in both superlayerss, but one of the 4-hit tracks has a

$\chi^2 > 2\ \mathrm{mm}^2$ and, according to the track definition, is "downgraded" to a 3-hit fit.

Figure 4 and Table 2 give the fraction of events in the different single-muon subsamples, separately for single-hit and multi-hit samples, and for the various angles of incidence.

Single-hit fits												
Muon	Angle (degrees)											
sample	-0.3	5.9	-10.7	11.4	14.1	19.1	-20.1	20.9	-28.8	30.9	32.6	42.5
4 + 4	74.1 ±0.2	65.0 ±0.2	68.0 ±0.2	70.2 ±0.3	73.0 ±0.3	77.8 ±0.2	76.3 ±0.2	79.3 ±0.3	77.0 ±0.2	78.5 ±0.2	78.0 ±0.3	54.3 ±0.4
4 + 3	18.9 ±0.2	30.4 ±0.2	29.7 ±0.2	26.6 ±0.3	22.4 ±0.3	20.9 ±0.2	21.9 ±0.2	19.3 ±0.3	21.3 ±0.2	20.1 ±0.2	20.5 ±0.3	39.7 ±0.4
3 + 3	1.5 ±0.1	4.6 ±0.1	2.3 ±0.1	3.2 ±0.1	4.6 ±0.1	1.3 ±0.1	1.7 ±0.1	1.3 ±0.1	1.7 ±0.1	1.4 ±0.1	1.4 ±0.1	6.0 ±0.2

Multi-hit fits												
Muon	Angle (degrees)											
sample	-0.3	5.9	-10.7	11.4	14.1	19.1	-20.1	20.9	-28.8	30.9	32.6	42.5
4 + 4	77.5 ±0.2	64.1 ±0.3	67.1 ±0.2	70.5 ±0.4	74.3 ±0.3	76.8 ±0.3	74.7 ±0.2	77.9 ±0.3	75.9 ±0.2	78.5 ±0.2	78.0 ±0.3	54.0 ±0.3
4 + 3	18.9 ±0.2	31.7 ±0.3	30.2 ±0.2	26.3 ±0.4	21.8 ±0.3	21.6 ±0.3	23.2 ±0.2	20.7 ±0.3	22.4 ±0.2	20.1 ±0.2	20.4 ±0.3	40.1 ±0.3
3 + 3	1.8 ±0.1	4.2 ±0.1	2.7 ±0.1	3.3 ±0.2	3.8 ±0.1	1.6 ±0.1	2.1 ±0.1	1.4 ±0.1	1.7 ±0.1	1.4 ±0.1	1.5 ±0.1	6.0 ±0.2

Table 2: Fraction of events (%) in the different single-muon subsamples depending on the number of hits participating in the track fit, for the various angles of incidence. The upper table is for single-hit fits and the lower table is for multi-hit fits.

The fraction of **4+4** tracks has a deep for $\sim 5^\circ$ and then increases with angle. The fraction of **4+3** tracks shows a complementary behaviour. It increases considerably when departing from normal incidence, reflecting the sudden increase of 3-hit fits at angles different from zero. This comes from the geometrical effect of I-beams. Two hits are lost for muons traversing this region at 0 degrees, and no fit is found. Ideally, it means that tracks will either be 4-hit fit or have no fit. At any other angle, this I-beam shadow effect is not produced and a set of natural 3-hit fits appears.

Notice that the fractions of events given in the first column of Table 2 (corresponding to 0°) do not sum up 100%. This is again because of the I-beam effect: The misssing fraction corresponds, precisely, to the muons crossing the I-beam region and having a 4-hit fit in one ϕ superlayer and no fit in the other (sample **4+x**). This sample amounts to (5.5 ± 0.1)% for single-hit fits and (1.9 ± 0.1)% for multi-hit fits. Departing from normal incidence the sample **4+x** no longer exists.

Also note that the **3+3** fraction is a very small in number.

3.1.1 Trigger Efficiency

In this section the global trigger efficiency as a function of the angle, and for the several single-muon subsamples defined in the previous section is studied.

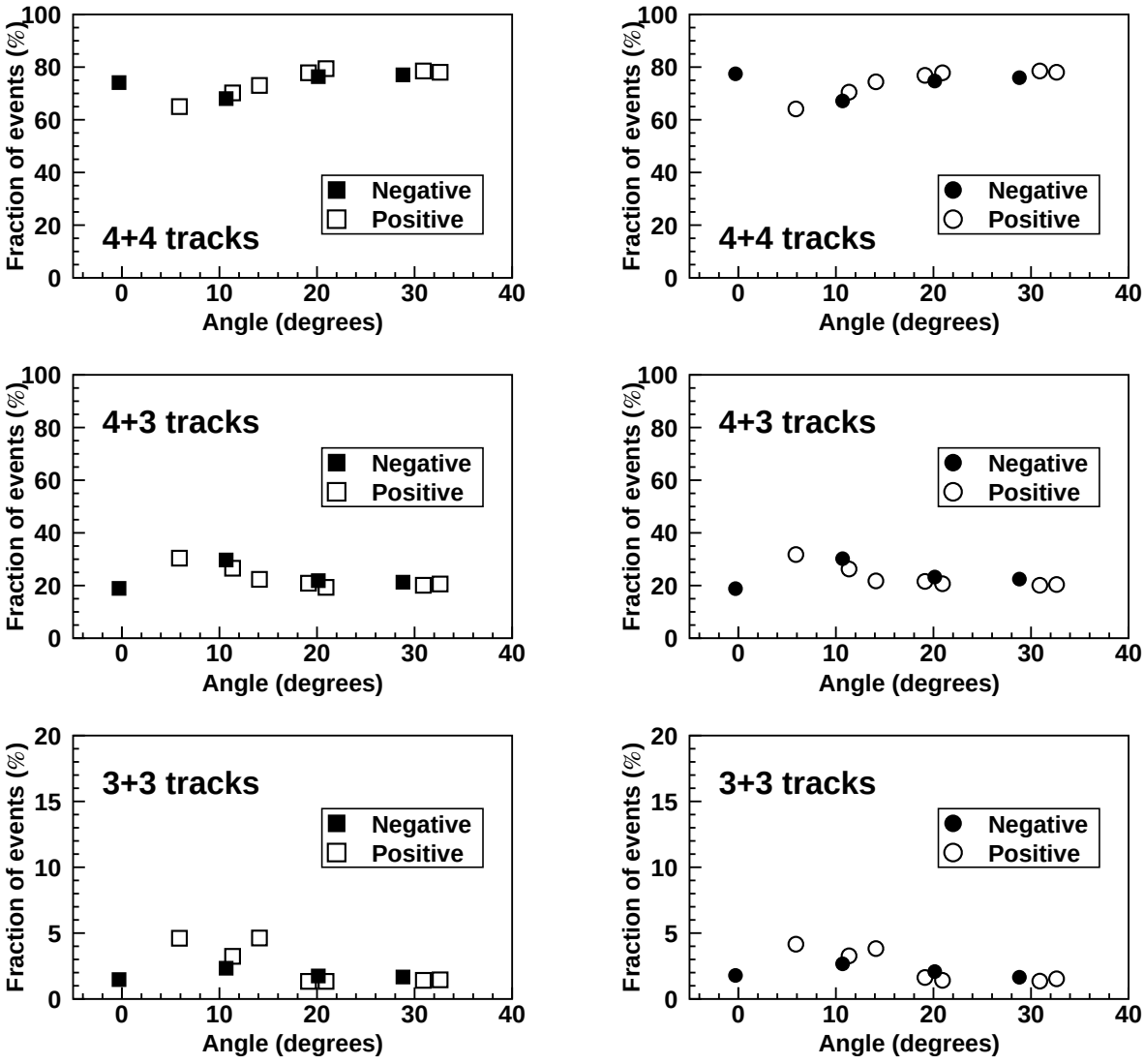

Figure 4: Fraction of events in the different single-muon subsamples as a function of the angle of incidence. Plots on the left (squared symbols) are for single-hit fits and plots on the right (circular symbols) are for multi-hit fits.

Global trigger efficiency is defined as the ratio of the number of events with any trigger information with respect to the total number of events in a given single-muon subsample (**4+4**, **4+3** or **3+3**). The global trigger efficiency for the different angles of incidence, is presented in Figure 5 and Table 3.

Single-hit fits												
Muon	Angle (degrees)											
sample	-0.3	5.9	-10.7	11.4	14.1	19.1	-20.1	20.9	-28.8	30.9	32.6	42.5
4 + 4	$100.00^{+0.00}_{-0.01}$	99.99 ± 0.01	$100.00^{+0.00}_{-0.01}$	$100.00^{+0.00}_{-0.02}$	99.99 ± 0.01	$100.00^{+0.00}_{-0.01}$	$99.99^{+0.00}_{-0.01}$	99.98 ± 0.01	99.98 ± 0.01	99.96 ± 0.01	99.83 ± 0.03	92.26 ± 0.30
4 + 3	99.92 ± 0.03	99.83 ± 0.04	99.80 ± 0.04	99.98 ± 0.02	99.90 ± 0.05	99.84 ± 0.05	99.67 ± 0.06	99.74 ± 0.08	99.42 ± 0.08	98.72 ± 0.11	98.27 ± 0.18	89.51 ± 0.40
3 + 3	90.53 ± 1.19	93.75 ± 0.58	91.32 ± 0.84	92.65 ± 1.10	93.35 ± 0.78	86.74 ± 1.64	84.72 ± 1.31	83.82 ± 2.23	82.69 ± 1.51	78.24 ± 1.52	76.86 ± 2.25	78.20 ± 1.40

Multi-hit fits												
Muon	Angle (degrees)											
sample	-0.3	5.9	-10.7	11.4	14.1	19.1	-20.1	20.9	-28.8	30.9	32.6	42.5
4 + 4	99.70 ± 0.03	99.83 ± 0.03	99.85 ± 0.02	99.86 ± 0.04	99.92 ± 0.02	99.77 ± 0.03	99.86 ± 0.02	99.80 ± 0.04	99.87 ± 0.02	99.75 ± 0.03	99.72 ± 0.04	90.54 ± 0.27
4 + 3	98.99 ± 0.12	99.22 ± 0.10	99.53 ± 0.06	99.39 ± 0.13	99.55 ± 0.10	98.91 ± 0.14	99.12 ± 0.10	98.95 ± 0.18	98.77 ± 0.12	98.18 ± 0.15	97.52 ± 0.23	89.35 ± 0.34
3 + 3	77.45 ± 1.64	89.83 ± 0.90	86.09 ± 1.06	90.95 ± 1.35	91.69 ± 1.04	78.74 ± 2.01	81.84 ± 1.44	85.24 ± 2.45	74.52 ± 1.75	73.63 ± 1.95	73.02 ± 2.40	78.06 ± 1.17

Table 3: Global trigger efficiency (%) as a function of the angle for the different single-muon subsamples. The upper table is for single-hit fits and the lower table is for multi-hit fits.

From the figures one concludes:

- The behaviour for single-hit and multi-hit cathegories is very similar, although the efficiency is somehow worse for the multi-hit sample, for the reason explained before.
- The global trigger efficiency is very high for all single-muon samples. It is virtually 100% for **4+4** and **4+3** samples. It only starts to deteriorate at $30°$.
- Even for **3+3** tracks, the global trigger efficiency is higher than 80% up to $20°$ and higher than 75% up to $35°$.
- The global efficiency for **4+x** tracks at $0°$ is $(98.2 \pm 0.8)\%$.

3.1.2 Event fractions with different Trigger Qualities

As it was stated in the begining, the aim of this study is to correlate the quality of the information provided by the trigger system, with the information given by the chamber, and in particular, with the quality of the reconstructed track. The working hypothesis is that a 4-hit fit will give a High Quality trigger, and a 3-hit fit will give a Low Quality trigger.

A **"better or equal than expected"** condition can be defined when the trigger performs as expected (or better, for completeness) as stated above, for a particular single-muon subsample. Therefore, the fraction of events with

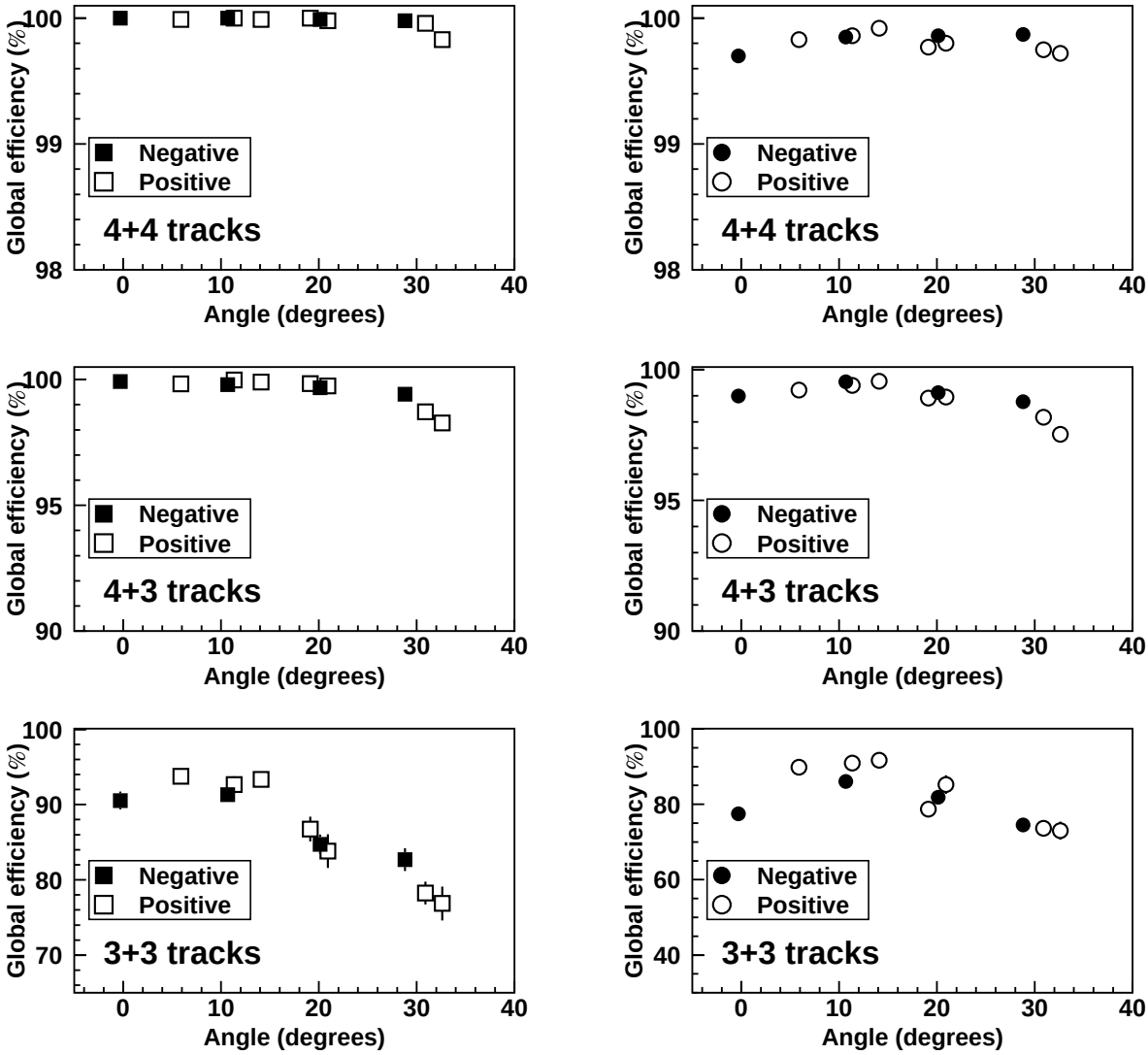

Figure 5: Global trigger efficiency as a function of the angle for the different single-muon subsamples. Plots on the left (squared symbols) are for single-hit fits and plots on the right (circular symbols) are for multi-hit fits.

trigger quality **"better or equal than expected"** can be evaluated, as the sum of the individual fractions for those trigger conditions better or equal to the "expected" one.

In the case of the $r-\phi$ view, track segments from two superlayers are available and the final "expected" trigger quality is the combination of the "expected" trigger qualities on both superlayers in the following way:

- Muon sample **4+4**.
  - Expected trigger level: HH.
  - "Better or equal than expected" condition: HH.
  - $\epsilon(\texttt{expected}) = \epsilon(\mathrm{HH})$
- Muon sample **4+3**.
  - Expected trigger level: HL.
  - "Better or equal than expected" condition: HL + HH.
  - $\epsilon(\texttt{expected}) = \epsilon(\mathrm{HL}) + \epsilon(\mathrm{HH})$
- Muon sample **3+3**.
  - Expected trigger level: LL.
  - "Better or equal than expected" condition: LL + HL + HH.
  - $\epsilon(\texttt{expected}) = \epsilon(\mathrm{LL}) + \epsilon(\mathrm{HL}) + \epsilon(\mathrm{HH})$

The fraction of events with the expected trigger quality as a function of the angle of incidence, is presented in Figure 6 and Table 4 for the different single-muon samples.

Muon sample 4+4:

The fraction of events with the expected trigger quality for single-hit **4+4** tracks (HH) is smoothly decreasing from 99% at 0° to 95% at 28.8°. It then suddenly drops for angles greater than 30°. This behaviour is already expected since it is related to the χ^2 distributions showed in Figure 3 where the fraction of tracks with a Low Quality trigger and $\chi^2 < 2$ mm^2, increased significantly from 28.8° to 30.9°.

Muon sample 4+3:

The fraction of events with the expected trigger quality for **4+3** cathegory (HL + HH) is considerably lower than in the **4+4** case. It starts at 75%, increases rapidly to 83% for 5° due to the I-beam effect, and gradually decreases to 51% at 33°.

Muon sample 3+3:

This sample behaves qualitatively very much like the **4+3** one. The fraction of events with the expected trigger quality (LL+ HL + HH) is 55% at 0°, increases to 77% for 5° and decreases again to 36% at 33°.

Numbers for multi-hit fits follow the same pattern.

To understand more deeply the evolution of the fraction of events with different trigger qualities as a function of the angle, Figure 7 and Table 5 give these fractions restricted to the angles of 0, 10, 20 and 30 degrees.

From Figure 7 and Table 5, the conclusions are:

Muon sample 4+4:

At normal incidence the fraction of events with the expected quality (HH) is almost 100%, the other contributions amount to less than 1%. Departing from normal incidence, the expected quality HH fraction decreases with the angle. This decrease translates into an increase of HL triggers. The fraction of HL events that was less than 1% (4.4%) at normal incidence reaches 9% (12.5%) at 33°, for single-hit (multi-hit) fits.

Single-hit fits												
Muon	Angle (degrees)											
sample	-0.3	5.9	-10.7	11.4	14.1	19.1	-20.1	20.9	-28.8	30.9	32.6	42.5
4 + 4	99.0	98.0	96.1	96.8	96.6	95.0	94.3	94.6	94.4	87.5	80.6	24.6
	±0.1	±0.1	±0.1	±0.2	±0.1	±0.1	±0.1	±0.2	±0.1	±0.2	±0.3	±0.5
4 + 3	75.2	83.3	81.6	75.1	67.0	62.0	66.6	58.0	60.1	51.2	51.5	25.6
	±0.5	±0.4	±0.3	±0.6	±0.7	±0.6	±0.5	±0.8	±0.6	±0.5	±0.7	±0.6
3 + 3	55.2	77.3	64.7	72.7	74.0	50.7	54.1	46.5	45.7	36.1	35.7	27.3
	±2.1	±1.0	±1.5	±2.0	±1.4	±2.6	±2.0	±3.3	±2.2	±2.0	±3.0	±1.7

Multi-hit fits												
Muon	Angle (degrees)											
sample	-0.3	5.9	-10.7	11.4	14.1	19.1	-20.1	20.9	-28.8	30.9	32.6	42.5
4 + 4	93.4	90.8	88.8	90.0	90.2	88.0	86.5	87.6	88.0	81.3	76.6	18.1
	±0.2	±0.2	±0.2	±0.3	±0.3	±0.2	±0.2	±0.3	±0.2	±0.2	±0.3	±0.4
4 + 3	65.9	76.5	74.9	66.3	59.6	58.0	62.6	55.5	52.8	46.3	50.1	18.1
	±0.6	±0.5	±0.4	±0.8	±0.8	±0.7	±0.5	±0.9	±0.6	±0.6	±0.8	±0.4
3 + 3	43.8	68.7	57.6	59.0	66.1	45.7	48.0	41.9	36.8	35.3	37.3	18.4
	±2.2	±1.5	±1.6	±2.4	±1.9	±2.8	±2.1	±3.7	±2.2	±2.5	±3.1	±1.2

Table 4: Fraction of events (%) with expected (better or equal) trigger quality as a function of the angle of incidence for the different single-muon samples. The upper table is for single-hit fits and the lower table is for multi-hit fits.

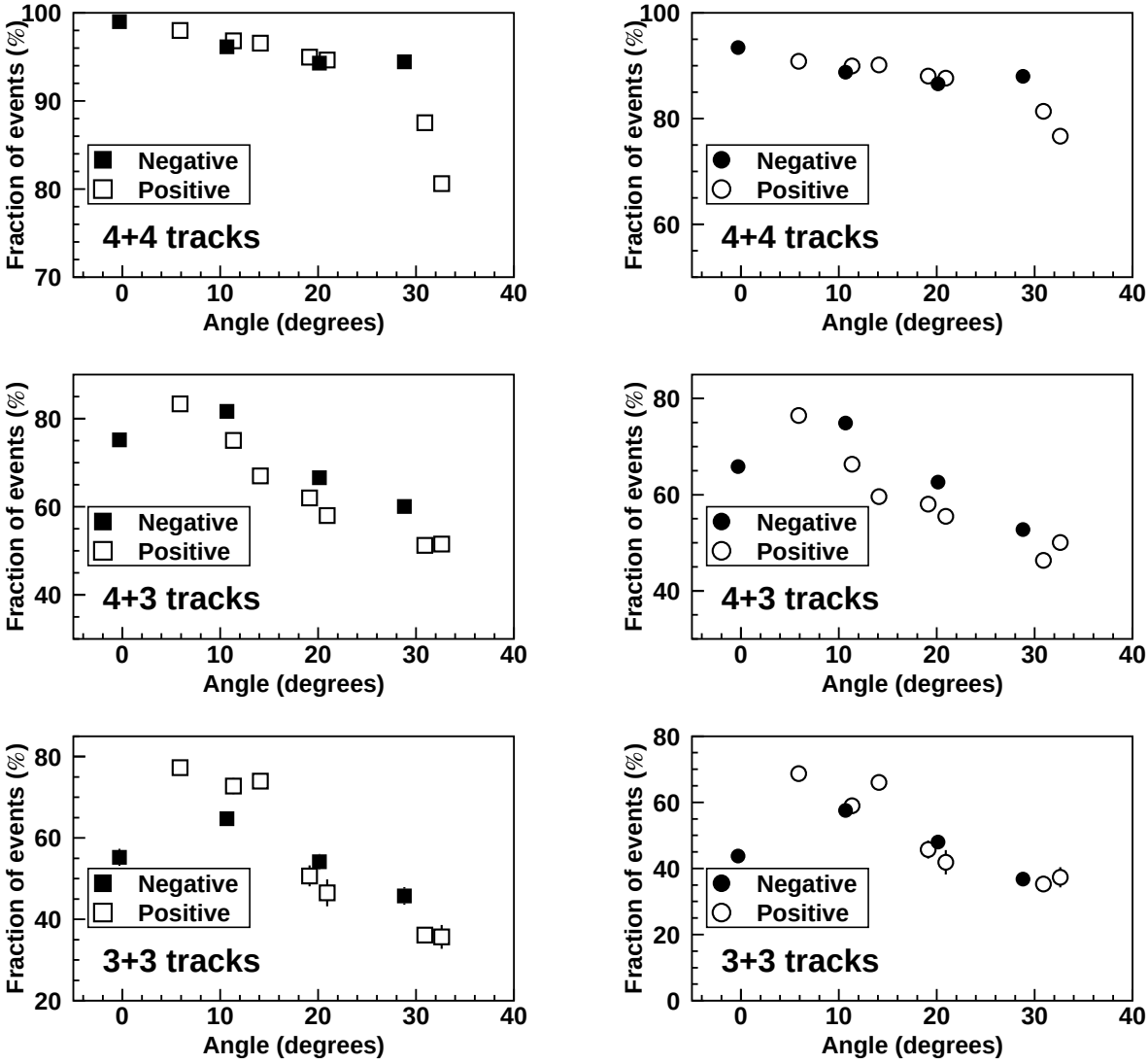

Figure 6: Fraction of events with expected (better or equal) trigger quality as a function of the angle of incidence for the different single-muon samples. Plots on the left (squared symbols) are for single-hit fits and plots on the right (circular symbols) are for multi-hit fits.

	Single-hit fits				**Multi-hit fits**			
	Muon sample 4+4				Muon sample 4+4			
Trigger	Angle (degrees)				Angle (degrees)			
quality	-0.3	11.4	19.1	30.9	-0.3	11.4	19.1	30.9
HH	99.0±0.1	96.8±0.2	95.0±0.1	87.5±0.2	93.4±0.1	90.0±0.3	88.0±0.2	81.3±0.2
HL	0.8±0.1	2.6±0.1	4.2±0.1	8.8±0.1	4.4±0.1	7.0±0.3	8.6±0.2	12.5±0.2
LL	$0.0^{+0.1}_{-0.0}$	$0.0^{+0.2}_{-0.0}$	$0.0^{+0.1}_{-0.0}$	0.2±0.1	0.1±0.1	0.2±0.1	0.1±0.1	0.4±0.1
H_o	0.1±0.1	0.2±0.1	0.4±0.1	2.1±0.1	0.7±0.1	1.0±0.1	1.3±0.1	2.9±0.1
H_i	0.1±0.1	0.2±0.1	0.4±0.1	1.2±0.1	1.4±0.1	1.8±0.1	1.8±0.1	2.5±0.1
L_o	$0.0^{+0.1}_{-0.0}$	$0.0^{+0.2}_{-0.0}$	$0.0^{+0.1}_{-0.0}$	0.1±0.1	$0.0^{+0.1}_{-0.0}$	$0.0^{+0.1}_{-0.0}$	0.1±0.1	0.2±0.1
L_i	$0.0^{+0.1}_{-0.0}$	$0.0^{+0.1}_{-0.0}$	$0.0^{+0.1}_{-0.0}$	0.1±0.1	0.1±0.1	0.1±0.1	0.1±0.1	0.2±0.1
No Trigger	$0.0^{+0.1}_{-0.0}$	$0.0^{+0.2}_{-0.0}$	$0.0^{+0.1}_{-0.0}$	$0.0^{+0.1}_{-0.0}$	0.3±0.1	0.1±0.1	0.2±0.1	0.2±0.1

	Muon sample 4+3				Muon sample 4+3			
Trigger	Angle (degrees)				Angle (degrees)			
quality	-0.3	11.4	19.1	30.9	-0.3	11.4	19.1	30.9
HH	2.6±0.2	1.0±0.1	1.5±0.1	2.7±0.2	2.6±0.2	1.1±0.2	1.9±0.2	2.5±0.2
HL	72.6±0.5	74.0±0.6	60.6±0.6	48.5±0.5	63.3±0.6	65.3±0.8	56.1±0.7	43.8±0.6
LL	0.4±0.1	2.2±0.2	1.2±0.1	2.3±0.1	2.1±0.2	4.6±0.3	2.7±0.2	3.1±0.2
H_o	9.9±0.3	10.0±0.4	15.1±0.4	20.0±0.4	10.6±0.4	11.2±0.5	15.4±0.5	20.0±0.5
H_i	14.4±0.4	12.3±0.5	20.4±0.5	23.2±0.4	19.8±0.5	15.2±0.6	21.0±0.6	25.4±0.5
L_o	0.1±0.1	0.1±0.1	0.4±0.1	1.3±0.1	0.4±0.1	1.0±0.2	0.9±0.1	2.0±0.2
L_i	0.1±0.1	0.4±0.1	0.9±0.1	2.0±0.1	1.2±0.1	1.7±0.2	1.8±0.2	3.1±0.2
No Trigger	0.1±0.1	0.0±0.1	0.2±0.1	1.3±0.1	1.0±0.1	0.6±0.1	1.1±0.1	1.8±0.2

	Muon sample 3+3				Muon sample 3+3			
Trigger	Angle (degrees)				Angle (degrees)			
quality	-0.3	11.4	19.1	30.9	-0.3	11.4	19.1	30.9
HH	0.6±0.3	0.4±0.3	0.5±0.4	$0.0^{+0.5}_{-0.0}$	0.2±0.2	0.2±0.2	1.2±0.6	0.5±0.4
HL	3.9±0.8	1.7±0.6	4.6±1.1	4.3±0.8	3.2±0.8	1.2±0.5	4.3±1.1	4.2±1.0
LL	50.8±2.1	70.6±2.0	45.6±2.6	31.8±1.9	40.4±2.2	57.5±2.4	40.2±2.7	30.5±2.4
H_o	0.6±0.3	0.2±0.2	1.3±0.6	1.6±0.5	0.8±0.4	0.2±0.2	1.5±0.7	1.3±0.6
H_i	0.6±0.3	0.4±0.3	0.8±0.5	0.3±0.2	1.0±0.4	0.5±0.3	1.2±0.6	2.1±0.7
L_o	13.9±1.5	10.4±1.3	14.7±1.8	23.5±1.8	20.8±1.8	13.6±1.7	15.3±2.0	25.5±2.2
L_i	29.7±2.0	16.2±1.6	32.4±2.4	38.5±2.0	33.7±2.1	26.7±2.2	36.2±2.7	35.8±2.5
No Trigger	9.5±1.2	7.3±1.1	13.3±1.6	21.8±1.5	22.5±1.6	9.1±1.3	21.3±2.0	26.4±1.9

Table 5: Fraction of events (%) with the different trigger qualities as a function of the angle of incidence. Left table is for single-hit fits and right table is for multi-hit fits.

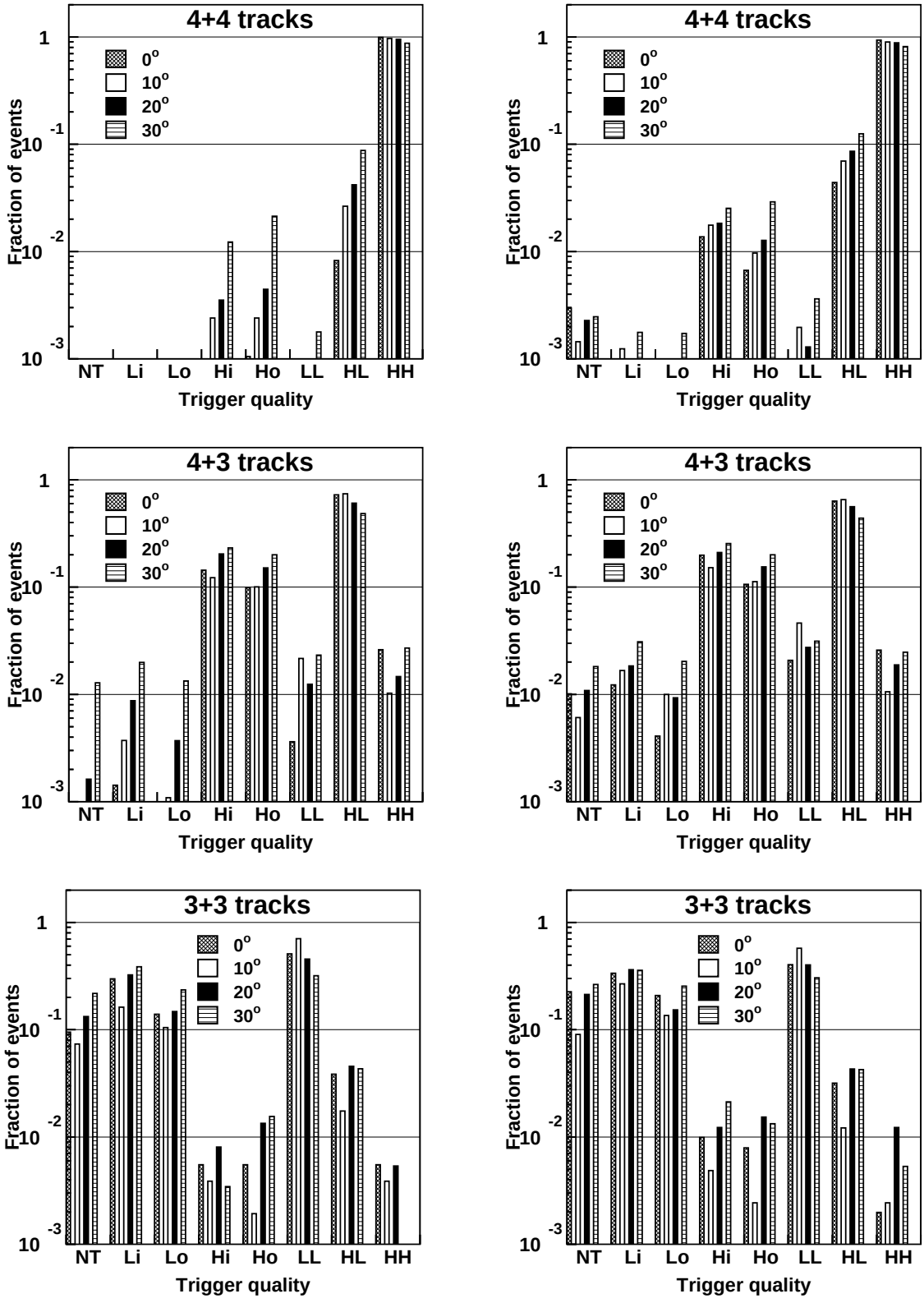

Figure 7: Fraction of events with the different trigger qualities, for normal incidence and at 10°, 20° and 30°. Plots on the left are for single-hit fits and plots on the right are for multi-hit fits.

Muon sample 4+3:

The expected trigger quality, HL amounts to $\sim 73\%$ at normal incidence, reaches a maximum at 10° and then decreases with the angle. Events in this cathegory migrate to $\mathrm{H_o}$ and $\mathrm{H_i}$ columns when the 3-hit segment is lost. One can notice two additional things: first, that there is a small fraction (2%) of HH triggers having a trigger quality better than expected. And second, that the fraction of $\mathrm{H_o}$ and $\mathrm{H_i}$ ($\sim 25\%$ at normal incidence increasing to $\sim 45\%$ at 30°) is considerably bigger than the LL cathegory. It means that a good 4-hit track in one superlayer, accompanied by another track in the other superlayer will ensure a High Quality trigger, and depending on the quality of the accompaning track one will have a correlated HL trigger or an uncorrelated high quality ($\mathrm{H_o}$ or $\mathrm{H_i}$) trigger.

Muon sample 3+3:

The expected cathegory, LL, is dominant, as expected. However, the fractions of events with $\mathrm{L_i}$ and $\mathrm{L_o}$ triggers are nearly as important, occurring when one of the 3-hit segments is not found. There is, even, a significant fraction of events with no trigger, when both segments are lost.

Conversely, it is important to note that virtually, all events with no trigger come from **3+3** tracks.

3.1.3 Resolution

A sample of single-muon events is selected, requiring a 4-hit track in SL-ϕ_1 and SL-ϕ_2, and having a High Quality trigger (HH).

From the comparison of the TRACO and chamber spatial information (taking into account the better chamber spatial resolution, ~ 300 μm) one obtains the TRACO spatial resolution (Figure 8, left, and Table 6). The TRACO angular resolution (Table 6) is obtained from the beam spot angular distribution as measured by the TRACO (Figure 8, right), once the beam angular dispersion (taken as 1 mrad) is removed.

Both resolutions are, approximately, constant with the angle: ~ 650 μm in position, and ~ 0.35 degrees for the angle.

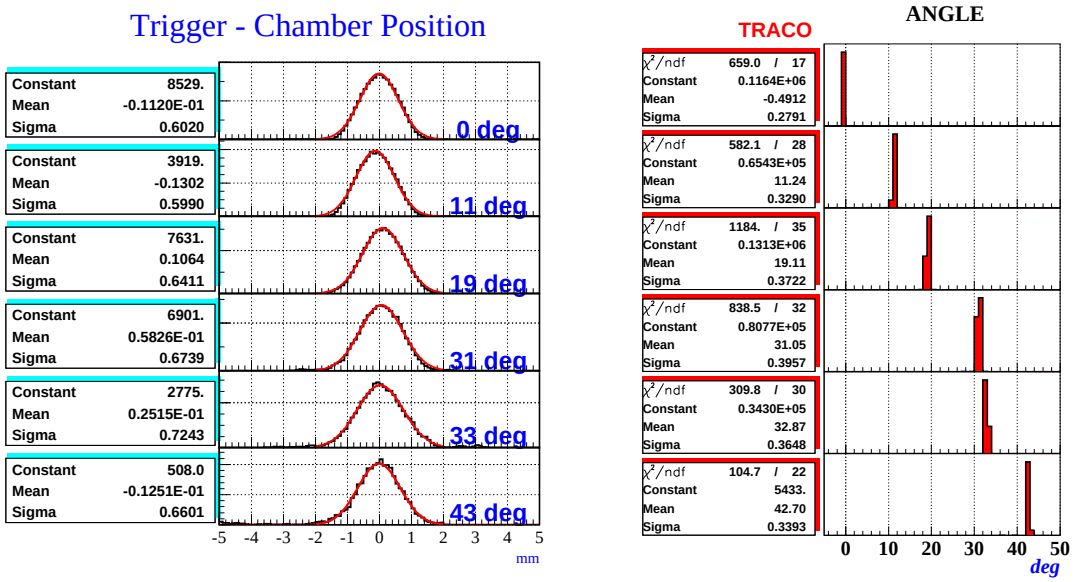

Figure 8: Left: Comparison of the TRACO and chamber track spatial information. Right: Incident beam angle measured by TRACO.

	Angle (degrees)					
	-0.3	11.3	19.1	30.9	32.6	43.0
Spatial resolution (mm)	0.60 $\pm$0.01	0.60 $\pm$0.01	0.64 $\pm$0.01	0.67 $\pm$0.01	0.72 $\pm$0.01	0.66 $\pm$0.01
Angular resolution (degrees)	0.27 $\pm$0.01	0.32 $\pm$0.01	0.37 $\pm$0.01	0.39 $\pm$0.01	0.36 $\pm$0.01	0.33 $\pm$0.01

Table 6: Spatial and angular track resolutions in TRACO for several incident beam angles.

3.2 θ Superlayer

The tracking algorithm presented in section 2 is also applied for tracks segments in superlayer θ. A High Quality trigger is expected for 4-hit tracks and a Low Quality trigger is expected for 3-hit tracks. Figure 9 shows the fraction of events with different trigger qualities for single-hit (left plot) and multi-hit (right plot) fits. The fraction of events with High Quality trigger is (98.84$\pm$0.04)% and the fraction of events with Low Quality trigger is (0.90$\pm$0.03)% for single-hit, and (92.83$\pm$0.14)% and (4.93$\pm$0.12)% for multi-hit fits, respectively. Notice that results for SL-θ refer to normal incidence, as it was not affected by the chamber rotation.

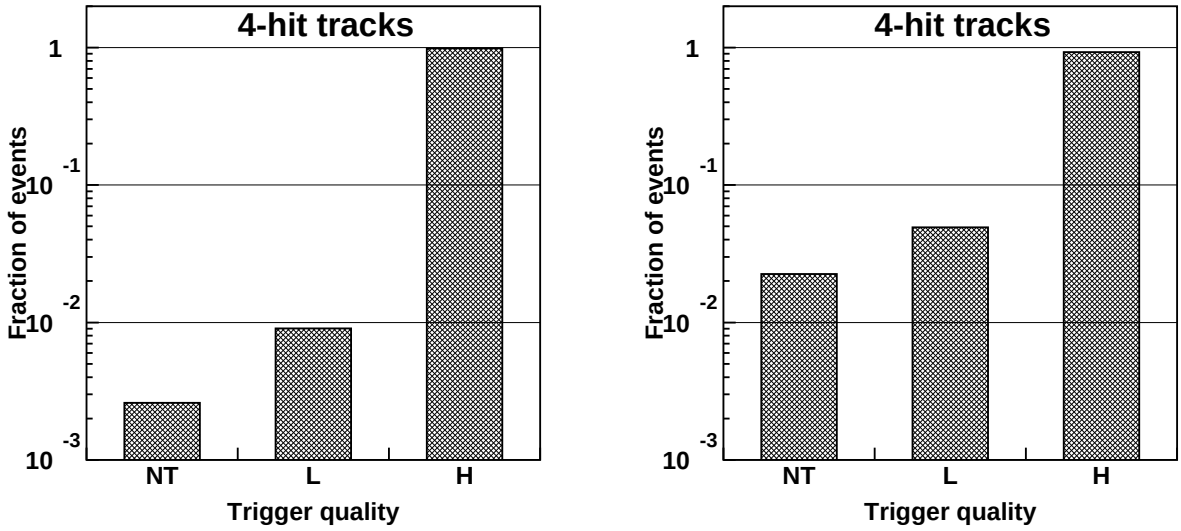

Figure 9: Fraction of events with different trigger qualities for the θ superlayer. The left plot is for single-hit fits and the right one is for multi-hit fits.

4 Di-muon trigger performance

The local DT Trigger system should be able to detect muon pairs when both muons cross the same station. When the DT local trigger finds two tracks coming from the same crossing (BX), the second track is recorded in the next cycle (BX+1). A flag indicates that it is a second muon of the previous BX. If a new muon is found at BX+1 the second muon track, previously recorded, is lost.

One has to take into account that the trigger system delivers, at most, two tracks after applying several algorithms to minimize trigger ambiguities. So, the second muon recorded in BX+1 may be a "real" one, as in the case of di-muons, or a "ghost" track generated artificially by the trigger system.

In this section we have studied the capability of the DT local trigger system to detect muon pairs crossing the same chamber at the same time.

For this study, a sample of "golden muon pairs" reconstructed in the chamber is selected: two muon tracks giving signal on the 4 layers of each ϕ SL and with a track fit-$\chi^2 < 2\ \mathrm{mm}^2$. To ensure that 2, and only 2, muons are crossing the chamber, events with 3 or more segments compatible with a muon pattern (3 or 4 hits, no matter the quality of the segment fit) in at least one ϕ SL, are excluded.

Di-muon pairs with the di-muon flag set by the trigger are further selected. Figure 10 shows, for these events, the spatial distance between the two muons computed from their reconstructed positions in the chamber *vs.* the distance between the muons computed from the information given by the trigger system. The correlation between them is very clean indicating that the muon pairs seen by the trigger and by the chamber reconstruction process are in fact the same.

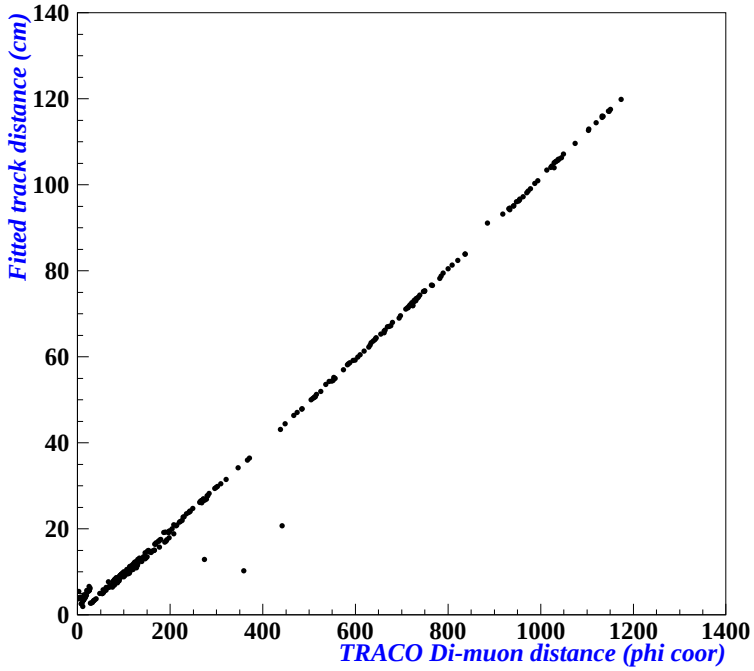

Figure 10: Di-muon distance measured by the chamber *vs.* di-muon distance from the trigger output.

The di-muon trigger efficiency is defined here as the ratio between the number of events where the trigger found both muons over the total number of di-muon events selected from the chamber information. The di-muon trigger efficiency is presented in Figure 11 as a function of the angle of incidence. It is $\sim 77\%$ at normal incidence, and increases with the angle reaching values bigger than 90%.

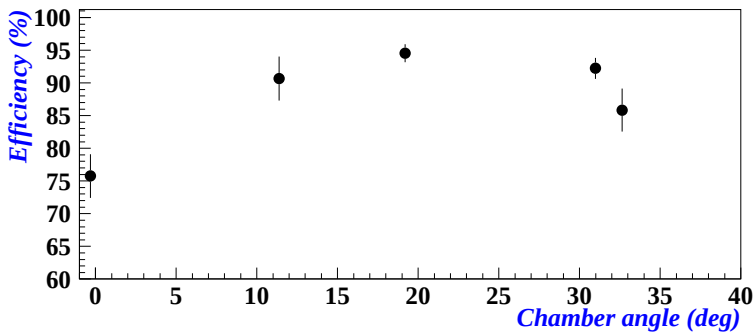

Figure 11: Di-muon trigger efficiency as a function of the angle of incidence.

The di-muon trigger efficiency as a function of the distance between the two muons was also evaluated. Figure 12 shows the results for 0 and 30 degrees incident angles. The distance between the two muons is given in terms of number of TRACOs. Within present statistics, no significant change in the di-muon trigger performance with the distance is observed.

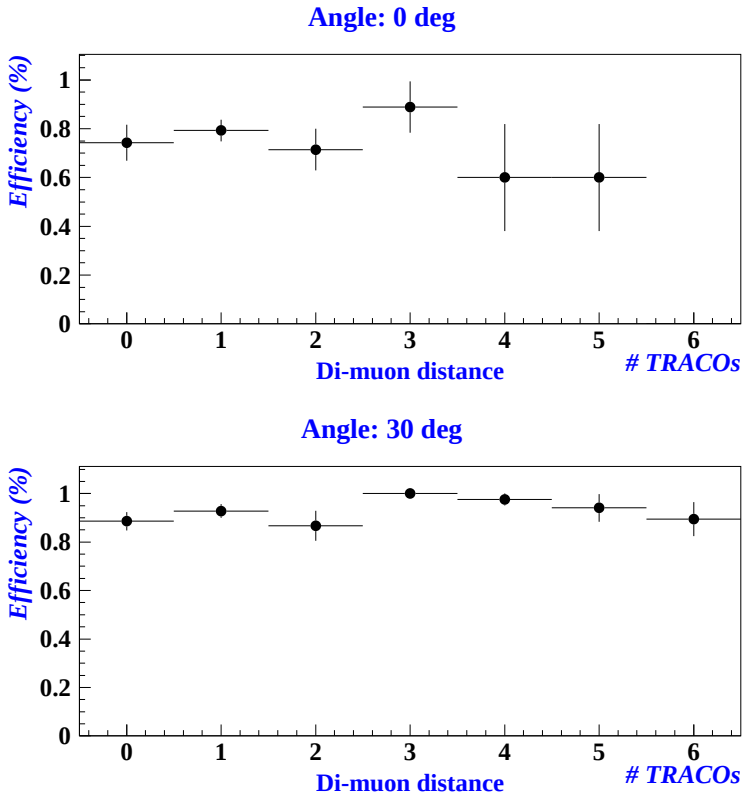

Figure 12: Di-muon trigger efficiency as a function of the distance between the two muons in terms of the number of TRACOs. The upper plot is for normal incidence and the lower plot for 30° incidence.

The trigger quality is now examined. Figure 13 shows, for the case of normal incidence, the trigger quality of the muons recorded in position BX (upper plot) and in position BX+1 (lower plot). The trigger quality for the two muons of the pair is, as expected, mostly HH.

5 Ghost studies

5.1 Ghost studies with di-muons

In the dimuon sample selected by applying the described criteria to the chamber data, there is a subsample of events that have not been identified as dimuons by the trigger system (the trigger di-muon flag is not set). A closer look at these events reveals that in most cases, the second muon is lost because the trigger found a muon from BX+1 crossing. The fraction of such events amounts to $\sim$ 18% (at normal incidence) of the initial set. Given the di-muon trigger efficiency of 77% (at normal incidence) presented in the previous section, one is left with an intrinsic di-muon trigger inefficiency of the order of 5%.

The trigger quality of this extra muon sample is presented in Figure 14. In most events the trigger is of low quality.

The spatial distance between the two muons computed from their reconstructed positions in the chamber *vs.* the distance of the muons computed from the information given by the trigger system, restricted to this sample where an extra muon is found, is shown in Figure 15 for normal incidence. Two groups of events can be observed: events where the extra muon has the same spatial position than the first muon triggered (di-muon distance in the

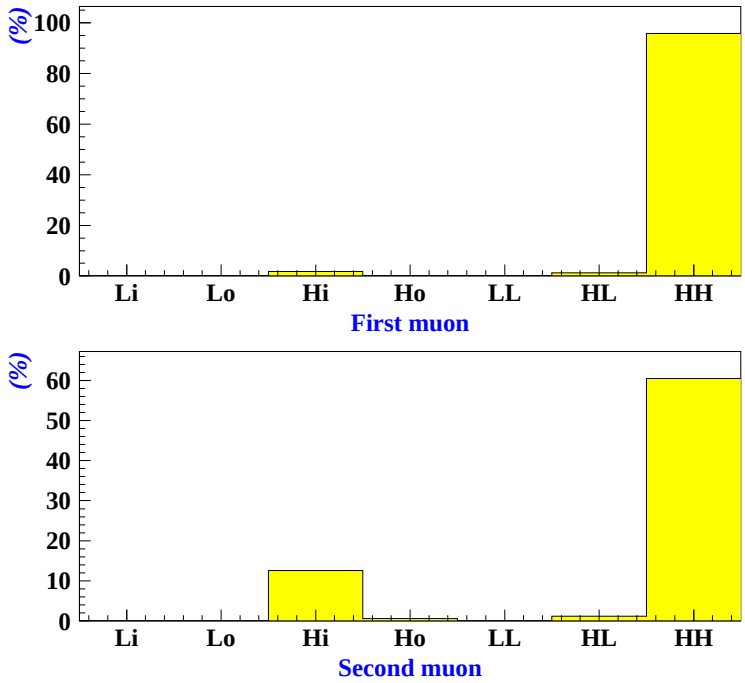

Figure 13: Fraction of di-muon events with the different trigger qualities (normal incidence). The upper plot is for the first muon in a crossing and the lower plot for the muon flagged as the second one of the same bunch crossing.

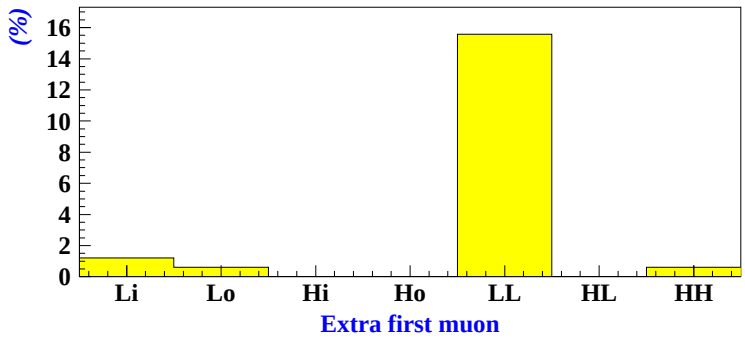

Figure 14: Fraction of chamber di-muon events with the various trigger qualities (normal incidence) for the muon found at BX+1 crossing.

trigger system is $\sim$ 0, independently of the di-muon distance measured in the chamber) and events where a good correlation between the di-muon distance measured from the trigger system and the distance measured by the chamber exists. Therefore, these muons recorded at BX+1, can be "identified" as ghost triggers of good muons.

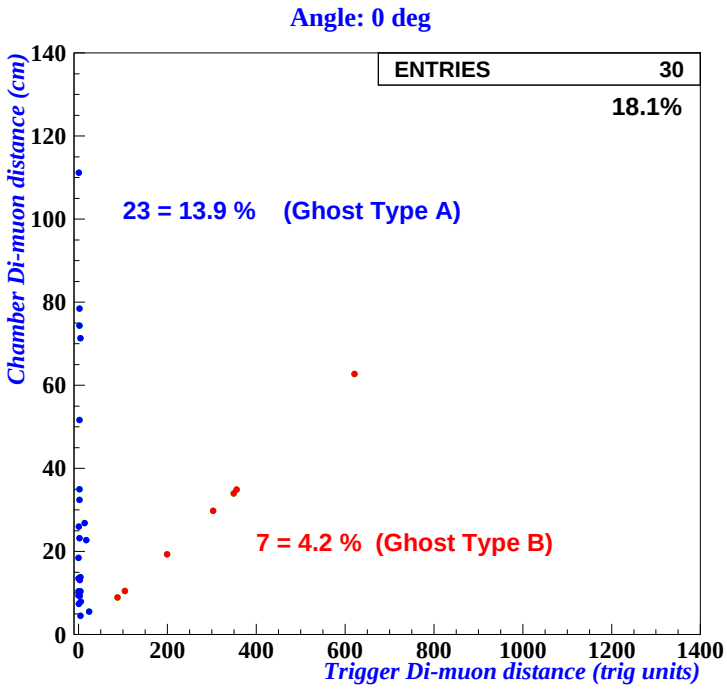

Figure 15: Di-muon distance measured in the chamber *vs.* the distance between the muons at BX and BX+1 slots recorded by the trigger, and for the sample at 0 degrees.

The first group, that amounts to 13.9% of events (over the total di-muon sample) can be identified as events where the extra muon is a ghost of the muon recorded in position BX. We will label this sample as **TYPE A** ghost.

The second group, where the di-muon distance from the trigger corresponds to the di-muon distance measured by the chamber amounts to 4.2% of the di-muon sample. In this case the extra muon triggered will be probably a ghost of the second muon of the pair. We will label this case as **TYPE B** ghost.

The sketch in Figure 16 illustrate the different possibilities of getting a ghost trigger.

The fraction of Type A and Type B events as a function of the angle of incidence is presented in Table 7. Type B fraction stays constant with the angle, about 5%, but Type A trigger rate decreases significantly from 13% at 0° to $\sim$1% departing from normal incidence.

Angle (degrees)	-0.3	11.4	19.1	30.9	32.6
Ghosts Type A (%)	13.9 ± 2.7	0.0 ± 2.3	0.4 ± 0.4	0.7 ± 0.5	1.8 ± 1.2
Ghosts Type B (%)	4.2 ± 1.6	8.0 ± 3.1	4.0 ± 1.2	4.6 ± 1.2	7.1 ± 2.4

Table 7: Fraction of di-muon events with ghosts on BX+1 slot as a function of the angle of incidence.

5.2 Ghost studies with single muons

Ghost triggers type A (a muon and its own ghost) must also be present in the single-muon sample. Profitting from the larger statistics of the single-muon sample, a dedicated study on ghost triggers induced by single-muons has

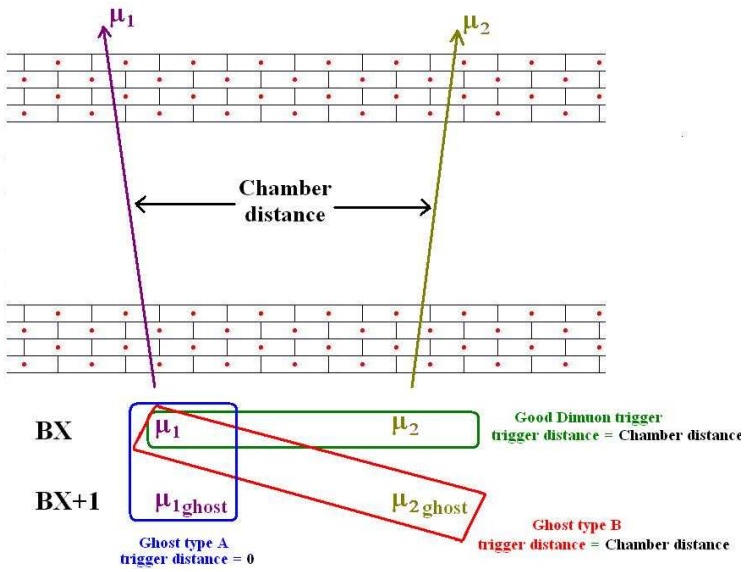

Figure 16: Sketch of the different trigger combinations found on the di-muon sample (see text).

been performed, and it is presented in this section.

A sample of single-muon events reconstructed in the chamber is selected with the same criteria than presented in the previous section. To ensure they are single-muon events, any event with two or more segments compatible with a muon pattern in at least one SL are excluded.

From the chamber single-muon sample, events with two muons found by the trigger are selected. One of them will be saved in BX position and another one in position BX+1. The muon recorded at BX+1 will be either flagged as a single muon of BX+1 crossing or as a second muon of BX crossing.

The trigger information on position for events with two single-muons found (one at BX and another one at BX+1 slots) indicates that both muons cross the chamber at the same point. Therefore they correspond to the same ghost triggers type A mentioned in the previous section. Table 8 shows the fraction of these events for the different angles of incidence. It shows a similar trend to what was observed in the di-muon sample (Table 7).

Angle (degrees)	-0.3	11.4	19.1	30.9	32.6
Ghost Type A (%)	8.7 ± 0.1	0.5 ± 0.1	0.8 ± 0.1	1.3 ± 0.1	3.0 ± 0.1

Table 8: Fraction of single-muon events with another muon on BX+1 slot, marked as single μ, as a function of the angle.

These Ghost triggers are a Low Quality duplicated of the first one and are due to the BTI overlap, as it can be seen in Figure 17 where it is shown the muon incident position, in the middle plate of SL-ϕ_1, for the sample where the trigger found another single muon on BX+1. The upper plot is for normal incidence and the lower plot for 30 degrees. At normal incidence two clear peaks are visible, that correspond to the position of borders of cells. At 30 degrees the number of Ghost events gets reduced and their position is more spread over the chamber and the peak structure is not so clear.

Finally, we have looked at the leftover events where the chamber had reconstructed one muon and the trigger had found two muons on the same crossing, recording one of them on BX slot and the other one on BX+1 slot, and the di-muon flag was set on. That is, they are single μ according to chamber but di-μ events from trigger criteria.

The trigger information showed that both muons cross the chamber at the same place, therefore the second muon is again a Ghost of the first one. Table 9 shows the fraction of these events as a function of the angle. This fraction is very low $\sim$1% at low angles and increases slightly at larger angles.

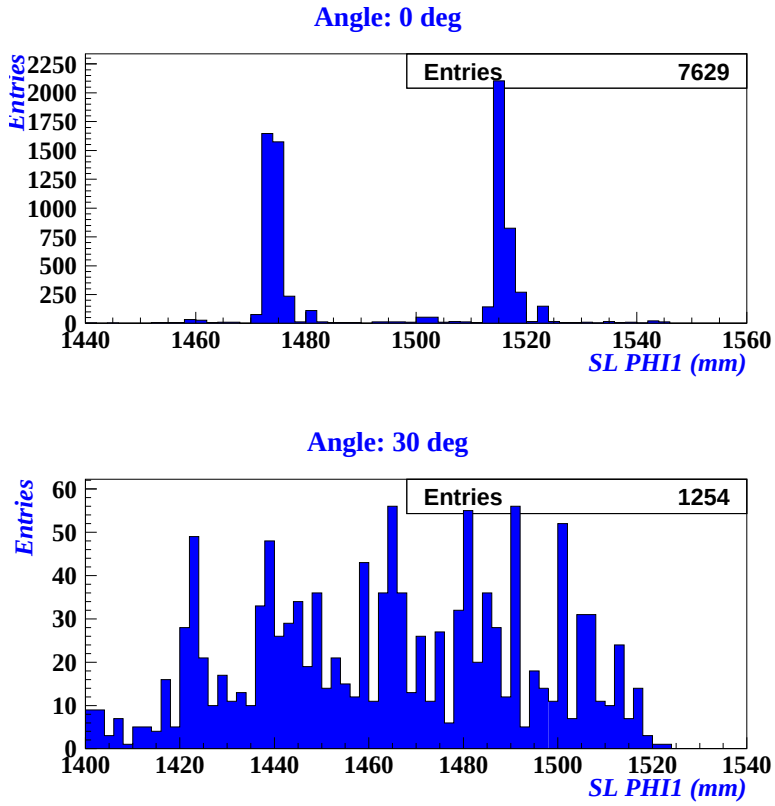

Figure 17: Muon incident position at SL ϕ_1 for events labelled as ghost Type A. The upper plot is for normal incidence, the lower plot for 30 degrees.

Angle (degrees)	-0.3	11.4	19.1	30.9	32.6
Ghost di-muon (%)	1.0 ± 0.1	0.2 ± 0.1	0.3 ± 0.1	2.6 ± 0.1	3.4 ± 0.1

Table 9: Fraction of single-muon events with another muon on BX+1 slot, and the di-muon flag set on, as a function of the angle.

Again we look for correlations between the position of the muon on the chamber and the probability of having a ghost. Figure 18 shows the muon position reconstructed in the chamber (in the middle plate of ϕ_1-SL). The upper plot is for normal incidence and the lower plot for 30 degrees. The peak structure is very clear in both cases. The peaks correspond to muons crossing the chamber through the border of the cells as it can be seen in Figure 19 where the lower plot of Figure 18 is splitted with different color codes depending on the cell border crossed. They are again due to the BTI overlap.

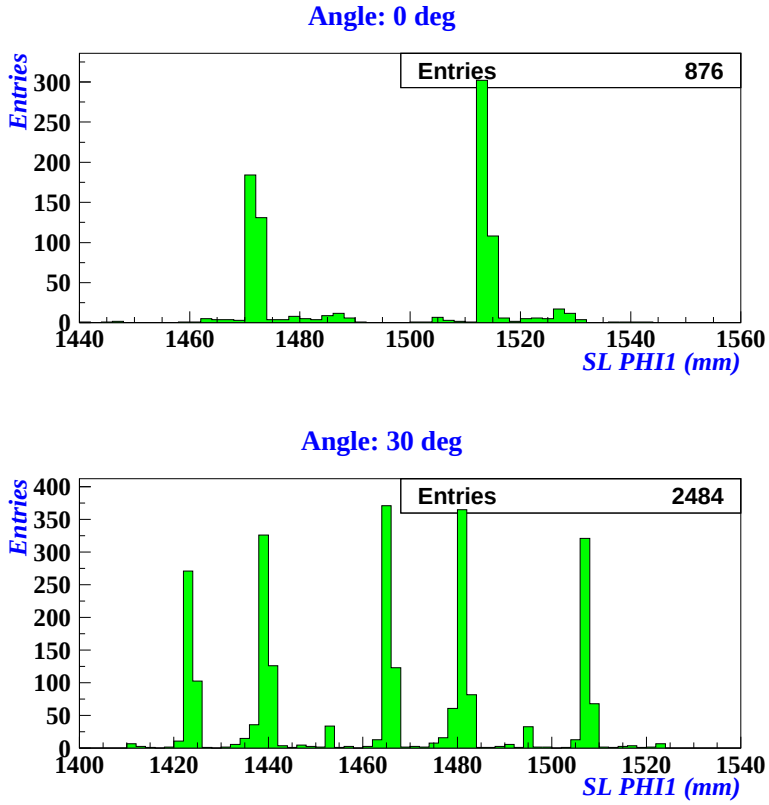

Figure 18: Muon incident position at SL ϕ_1 for events having a ghost di-muon trigger. The upper plot is for normal incidence, the lower plot for 30 degrees.

From this ghost study one concludes that Ghost triggers are significant only at $0°$. Changes in the parameters of the ghost rejection procedure would decrease the level of ghosts but at the price of a reduction in the single muon trigger efficiency [1].

6 Conclusions

The analysis of the May 2003 test beam data has provided a very complete set of results which fully validate the local DT muon trigger performance. We have presented in this note a partial view of these results, following the approach of comparing the DT chamber readout information with the response given by the trigger. For single muons, the trigger efficiency and the trigger spatial and angular resolutions have been obtained for different cathegories of events, and as a function of the beam angle of incidence.

The expected correlation between reconstructed tracks and single muon triggers of different qualities has been established in all cases using a single cut for the fit-χ^2 at $\chi^2 < 2$ mm^2. Four-hit segments are always recognized by the BTI, and the TRACO correlates them successfully at all angles of incidence up to $30°$. On the contrary, for 3-hit tracks, the BTI fails sometimes to recognize them and the TRACO is not always able to correlate them.

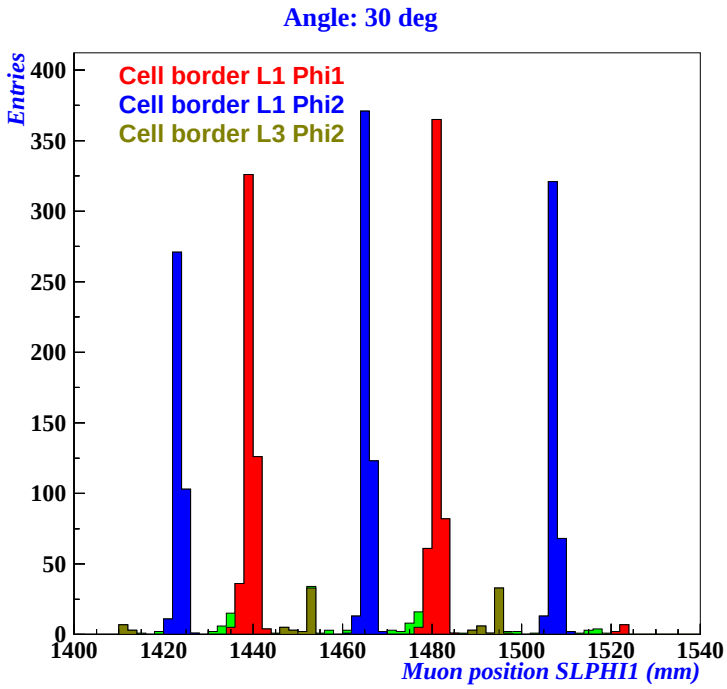

Figure 19: Muon incident position at SL ϕ_1 for events having a ghost di-muon trigger. The angle of incidence is 30 degrees. The different colors indicate different chamber regions.

Degradation of the trigger system performance starts at smaller angles of incidence.

The dimuon trigger performance has also been studied. Some special cases of ghost triggers have been evaluated and understood.

References

[1] P. Arce et al. *Bunched Beam Test of the CMS Drift Tubes Local Muon Trigger*. Accepted by Nucl. Instrum. and Meth. in Physics Research A.

[2] C. Albajar et al. *Test Beam analysis of the first CMS Drift Tube Muon Chamber*. Nucl. Instrum. and Meth. in Physics Research A 525 (2004) 465.

[3] B. de la Cruz et al., *Results on 2003 Testbeam*, Talk at the Muon-DT session. December 2003 CMS week. `http://wwwae.ciemat.es/cms/talks/cmsweek_dec03/testbeam_03.pdf`.